INSTITUTE OF PHYSICS PUBLISHING INVERSE PROBLEMS

Inverse Problems **17** (2001) 1597–1610 PII: S0266-5611(01)23748-4

Linear and nonlinear iterative scalar inversion of multi-frequency multi-bistatic experimental electromagnetic scattering data

René Marklein, Kannan Balasubramanian, Anyong Qing and Karl J Langenberg

Electromagnetic Field Theory, Department of Electrical Engineering, University of Kassel, D-34109 Kassel, Germany

E-mail: marklein@uni-kassel.de, kbalasub@uni-kassel.de, ayqing@uni-kassel.de and langenberg@uni-kassel.de

Received 9 April 2001
Published 13 November 2001
Online at stacks.iop.org/IP/17/1597

Abstract

This paper reports results obtained by linear and nonlinear iterative scalar inversion of experimental electromagnetic scattering data sets for different targets. The applied inversion schemes are a linear diffraction tomography algorithm and three nonlinear iterative methods. Two domain integral equation based methods, namely a modified gradient in field algorithm and a contrast source inversion method, are used. The third method is a real-coded genetic algorithm based on a boundary integral equation formulation. Inversion results are presented and compared for dielectric targets (penetrable scatterers) and metallic targets (perfect scatterers) using measurements for the transverse magnetic polarization case acquired in an anechoic chamber.

1. Introduction and overview of the applied inversion schemes

Inverse scattering algorithms are usually validated against synthetic data; here, 2D experimental data are available: multiple frequency angular diversity bistatic data. We apply all the algorithms presently available to us, so this paper is, within this special section, a subset of comparisons of linearized and nonlinear iterative scalar inversion methods:

(i) diffraction tomography (DT) algorithm,
(ii) modified gradient in field (MGF) method,
(iii) contrast source inversion (CSI) method,
(iv) real-coded genetic algorithm (RGA).

Table 1. Parameters of the processed data sets (see Sabouroux and Pezin (2000)).

Target	Data set	Polarization	Frequency band in GHz	Frequency step in GHz
Single circular dielectric cylinder	dielTM_dec8f.exp	TM	1–8	1
Two circular dielectric cylinders	twodielTM_dec8f.exp	TM	1–8	1
Centred rectangular metallic cylinder	rectTM_cent.exp	TM	4–16	4
Decentred rectangular metallic cylinder	rectTM_dece.exp	TM	2–16	2
U-shaped metallic cylinder	uTM_shaped.exp	TM	2–16	2

Nonlinear iterative algorithms differ a great deal regarding having to solve the direct problem or not, modelling the scatterer, global versus local, accuracy, convergence, effectiveness; hence, it might be useful to have a comparison out of one laboratory only.

For example, we have chosen as conjugate gradient (CG) based (local) iterative optimization schemes a modified gradient and a contrast source inversion method and as a representative for a global optimization scheme the real-coded genetic algorithm.

Measured electromagnetic scattering data sets in the gigahertz (GHz) regime have been obtained from experiments performed in an anechoic chamber for five different objects: a single and two identical circular dielectric cylinders, a centred and a decentred rectangular metallic cylinder and a U-shaped metallic cylinder (see table 1). For these objects time-harmonic multi-frequency multi-bistatic data are measured at 49 receiver positions on a circle with a radius of 760 ± 3 mm and for 36 different emitter positions on a circle with a radius of 720 ± 3 mm around the target. Relative to a fixed emitting antenna at 0° the receiving antenna is rotated in a limited angular range from 60° to 300° with a 5° stepping ($\propto$ 49 positions) and the target is rotated in the full range from 0° to 350° with a 10° stepping ($\propto$ 36 positions).

A detailed description of the underlying experimental setup as well as the data sets is given in the introduction by Belkebir and Saillard (2001) to this special section (see also Sabouroux and Parneix (1992), Belkebir *et al* (2000) and Sabouroux and Pezin (2000)). Throughout the paper only the data sets for the transverse magnetic (TM_z) polarization are processed. The data sets under consideration are collected in table 1.

The objects for which experimental scattering data have been provided can be classified into two groups:

(i) (homogeneous) dielectric targets,
(ii) metallic targets.

For these two types of scatterers the inverse scattering problem is to reconstruct the following parameters:

- (homogeneous) dielectric targets: shape, position and relative permittivity of the target;
- metallic targets: shape and position of the target.

Since *a priori* information of the dielectric and metallic scatterer types are known, these can be used to derive inversion schemes which are matched to the type of scatterer under consideration. The applied algorithms are sketched in the following subsections and in the next section the inversion results are presented and discussed.

1.1. Linear diffraction tomography algorithm

The applied linear scalar DT algorithm solves the linearized Porter–Bojarski integral equation using the first-order Born approximation utilizing K-space calculus. If we assume a monochromatic plane wave as the incident field we can formulate a 'near'-field angular diversity DT inversion scheme for the 'band-limited' contrast function. We note that in angular diversity mode the algorithm processes a single frequency only. For a circular measurement surface a fast algorithm can be formulated applying only fast Fourier transforms (FFT) to compute the Fourier series and Fourier transforms. The following steps are processed in angular diversity mode for a fixed frequency in the 2D case:

(i) Compute the scattering amplitude by performing a near-field to far-field transformation of the measured scattering data. For a circular measurement circle this can be executed by the following sequence: (i) perform a 1D FFT with respect to the observation angle, (ii) multiply a near-field to far-field filter function, (iii) compute an inverse 1D FFT with respect to the integer order n.
(ii) Apply the so-called K-space mapping, which puts the far-field data in the form of the scattering amplitude on the corresponding eccentric singular Ewald circle in K-space.
(iii) In angular diversity mode the above steps are computed for each angle of incidence (emitter position) which 'clears' the null space in K-space—'fills up' the K-space—of the contrast function.
(iv) Compute a 2D inverse Fourier transform with respect to the position vector in K-space which gives the contrast function in the r-space.

In all inversion examples we use an FFT with a length of 64 for the Fourier series computation in the near-field to far-field transformation and a two-dimensional uniform grid of 512×512 subsquares for the inverse 2D FFT. The DT algorithm has been coded to handle a number of receivers (the number must be a power of two), an arbitrary number of emitters and frequencies in single frequency mode. We note that we apply the above Born-type DT algorithm to non-Born-type targets as well.

For further details of the algorithm and implementation we refer to Langenberg (1987, 2001), Morbitzer (1991) and Hofmann (1999).

1.2. Modified gradient in field method

In the MGF method, which was first introduced by Kleinman and van den Berg (1992), the inverse problem is posed as an optimization problem where a scalar cost functional is minimized by a nonlinear iterative CG based scheme. The scalar cost functional is a sum of the defects in the data and domain integral equation. In MGF the unknowns are the total field and the contrast function (material contrast), both being in general complex functions. The updates of the unknowns are computed simultaneously at each iteration step using two CG methods running concurrently. This approach avoids the necessity to solve the forward problem in each iteration step. The MGF algorithm has been implemented to handle an arbitrary number of receivers, emitters and frequencies, simultaneously.

Since *a priori* information about the targets is available, two different versions of MGF are utilized. For dielectric targets we apply the standard MGF method, while for metallic (conducting) targets we apply a modified scheme which we call MGFM, i.e. MGF for metallic scatterers as suggested by Kleinman and van den Berg (1994).

For the dielectric case, we always assume a purely real material contrast, i.e. $\chi = \varepsilon_r - 1$, where ε_r is the relative permittivity of the homogeneous dielectric object. For metallic scatterers we always assume a purely imaginary material contrast, i.e. $\chi = j\zeta^2$, where ζ is real-valued

and replaces the contrast as the second unknown in the iterative process, wherein a maximum value for ζ is imposed while the iterative process is running. For all the algorithms mentioned here, the incident field has been assumed to be a monochromatic plane wave.

In such iterative algorithms the initial guess considered for the unknown field quantities plays a crucial role in the convergence of the method. One very obvious initial guess is to have zero contrast and the initial total field set to the incident field. Another possibility is the so-called backpropagated contrast obtained by an initial contrast source minimization as used by Kleinman and van den Berg (1994). As discussed in the results, it has been found that the convergence is faster with the backpropagated contrast as the initial guess. Hence, this has been used as the initial guess throughout.

Two kinds of multi-frequency approaches are possible. In the first approach, called the concurrent frequency mode, data pertaining to more than one frequency are used simultaneously in every iteration step of the algorithm. In the second approach, called frequency-hopping mode, the algorithm is first run for the lowest frequency and the resulting reconstruction is then used as the initial guess for the next run using the next higher frequency, and so on, until the highest frequency is reached.

For the dielectric objects the reconstruction space has a size of 150 mm $\times$ 150 mm represented by a uniform grid of 64 $\times$ 64 subsquares. MGF is run for 64 iterations for the frequencies of 1, 2, 3 and 4 GHz in the concurrent mode. In the conducting case for metallic scatterers a uniform grid of 64 $\times$ 64 subsquares representing a domain of 75 mm $\times$ 75 mm is used. MGFM is run for 64 iterations in frequency-hopping mode using four frequencies 4, 8, 12 and 16 GHz.

A detailed description of the MGF can be found in Kleinman and van den Berg (1992, 1994), van den Berg (1999, 2001) and Haak (1999).

1.3. Contrast source inversion method

In the CSI method proposed by Kleinman and van den Berg (1997) the unknown field quantities are the contrast source and the material contrast. Here, the contrast source is the product of the material contrast and the total field. The CSI method is, like the MGF, an iterative algorithm comprising the following three main steps in every iteration:

(i) Computation of the contrast source by minimization of the scalar cost functional given by the integrated misfit of the data and domain integral equation.
(ii) Calculation of the total field in the scatterer by substituting the contrast source approximation in the object representation.
(iii) Reconstruction of the object function by minimization of a scalar functional which is a global representation of the misfit in the domain integral equation.

A variant of the CSI is derived by using weighted contrast sources where the contrast source and the total field are weighted by the incident field. We call this method in brief CSIW. It has been observed that the CSIW performs better than the CSI, as is also known from the work by Haak (1999). Hence, the CSIW is used in the results reported in the next section. CSI and CSIW have been implemented to handle an arbitrary number of receivers, emitters and frequencies simultaneously. As the initial value we again select the backpropagated contrast over the entire region as used before for the MGF method in the previous subsection.

The CSIW is run with *a priori* information. For dielectric targets a purely real material contrast and for metallic objects a purely imaginary material contrast is assumed. The constraint of positivity, as given by Haak (1999), is not imposed. The concurrent approach using frequencies of 1, 2, 3 and 4 GHz is followed for the dielectric objects. In all examples a

search area of 150 mm × 150 mm is selected and discretized with a uniform grid of 64 × 64 subsquares.

For the metallic targets, in contrast to MGFM, no maximum value is imposed for the imaginary part of the contrast during the iterative process. The frequency-hopping mode for the frequencies 4, 8, 12 and 16 GHz is applied for the metallic targets. A reconstruction space of 75 mm × 75 mm is used in the metallic case which is discretized by a uniform grid of 64 × 64 subsquares. The CSIW is run for a maximum of 200 iterations for the dielectric and 128 iterations for the metallic case.

A detailed description of the CSI can be found in Kleinman and van den Berg (1997), van den Berg (1999, 2001) and Haak (1999).

1.4. Real-coded genetic algorithm

The RGA is a global optimization tool similar to others, such as the neural network, the simulated annealing, the evolution strategy and the Monte Carlo method. For the application of the RGA in inverse scattering the problem is cast into a global optimization problem by optimizing a scalar cost functional. The scalar cost functional is proportional to the misfit in the measured and predicted field. Note that the predicted field is computed by solving the forward problem at each iteration step, which is one of the bottlenecks in this algorithm. In the RGA the following steps are performed for the optimization of the cost functional:

(i) Initialization with a randomly generated initial population of individuals within a finite search space. The population size is 300 throughout the paper. Now the iterative procedure of the RGA is started which comprises the preprocessing, three genetic operations and the postprocessing.
(ii) In the preprocessing stage a scaling operator is applied to scale the object function into an appropriate fitness function.
(iii) Then, the first genetic step in terms of the selection operation is performed, which selects good members among the population into the mating pool on the basis of their fitness function. Common selection rules are roulette-wheel, ranking and stochastic binary tournament, with the latter used throughout in these examples.
(iv) In the second stage, the crossover operation as the main search tool of the RGA is executed. After mating two parent members new temporary members are generated by crossing over the mated pairs with a certain probability.
(v) The final genetic operation is the mutation which generates a new population.
(vi) The elitist model as a postprocessor avoids convergence problems, where the worst member of the new population is replaced by the best member in the previous population.

The above iteration process goes on until an acceptable solution is achieved. The implemented RGA can process multi-bistatic data sets in single frequency mode and can handle (homogeneous) dielectric and metallic scattering targets. A boundary integral equation formulation is used for the computation of the forward problem. The shape function is represented by a cubic B-spline approximation using 6 control points. Further details are given by Qing (2001), Qing and Lee (1999), Qing and Zhong (1998) and Qing *et al* (2001).

2. Inversion results

This section presents the inversion results for the dielectric and metallic targets summarized in table 1 using the inversion parameters collected in table 2. The targets are embedded in a free-space environment. The operation frequencies and corresponding wavelengths for the free-space background are given in table 3.

Table 2. Parameters of the processed data sets. BP: backpropagation; DI: dielectric; ME: metallic; PW: plane wave; SF: single frequency; CF: concurrent frequencies; FH: frequency-hopping.

Inversion scheme	DT	MGF	MGFM	CSIW	RGA
Targets applied	DI/ME	DI	ME	DI/ME	DI/ME
Initial guess	—	BP	BP	BP	—
Number of iterations	—	64	64	200/128	20–40
Computational times[a]	<1 s[b]	4 h[c]	4 h[c]	4 h[c]	24 h[b]
Incident field	PW	PW	PW	PW	PW
Frequency approach and applied frequencies in GHz	SF: 8 and 16	CF: 1, 2, 3 and 4	FH: 4, 8, 12 and 16	CF: 1, 2, 3 and 4 FH: 4, 8, 12 and 16	SF: 8 and 16
Figure	1–5(*b*)	1–2(*c*)	3–5(*c*)	1–5(*d*)	1(*e*), 3(*e*), 4(*e*)

[a] On a MIPS R10K 2.6 processor machine.
[b] Computational time for one frequency.
[c] In the concurrent frequency (CF) and frequency-hopping (FH) mode in total four different frequencies are processed simultaneously. The computational time is the total elapsed time needed for all frequencies.

Table 3. Measurement frequency and corresponding wavelength in the background (free space with the speed of light $c_0 \approx 3 \times 10^8$ m s^{-1}).

Frequency in GHz	1	2	3	4	8	12	16
Free-space (background) wavelength in mm	300	150	100	75	37.5	25	18.75

2.1. Single circular dielectric cylinder

The first example, given in figure 1(*a*), is a single circular dielectric cylinder with a diameter of $D = 30$ mm and the centre on the y axis at $y = 28$ mm and has a relative permittivity of $\varepsilon_r = 3 \pm 0.3$, corresponding to a real-valued material contrast of $\chi = 2 \pm 0.3$. The dielectric permittivity has been measured using a waveguide technique (Sabouroux and Parneix 1992). Figures 1(*b*)–(*e*) display the results for the linear DT scheme, the MGF method, the CSIW method and the RGA. The reconstruction of the linear DT scheme using a single frequency of 8 GHz is shown in figure 1(*b*), where 8 GHz correspond to a free-space wavelength of $\lambda = 37.5$ mm and a diameter-to-wavelength ratio of $D/\lambda = 0.8$. Shape and position are clearly visible. The reconstructed maximal contrast is too high with $\chi = 2.7$ and the cylinder appears slightly shifted to the right. Figure 1(*c*) displays the MGF result of the reconstructed material contrast using the backpropagated contrast as the initial guess and the first four frequencies 1, 2, 3 and 4 GHz in the concurrent multi-frequency mode. One can recognize that the MGF result for 1, 2, 3 and 4 GHz is comparable to the 8 GHz-DT result, while the reconstructed maximal material contrast of $\chi = 2.4$ using the MGF is slightly above the tolerance. The CSIW result also obtained in the concurrent multi-frequency mode for 1, 2, 3 and 4 GHz reproduces the actual cylinder very well and the retrieved maximal contrast of $\chi = 1.9$ is within the given tolerance. In contrast to the CSIW result a weak ringing is visible in the DT and MGF results. The RGA result for a single frequency of 8 GHz is shown in figure 1(*e*). This result represents the retrieved contour, which is, as for the DT result in figure 1(*b*), a little shifted to the right. The value of the reconstructed contrast is $\chi = 2.3$ and is, like the CSIW result, within the given tolerance. Obviously, the CSIW and RGA results are superior to the MGF and DT results. The computational time of the linear DT scheme for a single frequency

is less than one second, quasi real-time imaging, while the MGF and CSIW needs four hours in the multi-frequency mode and the RGA in the single frequency mode needs approximately twenty-four hours on a MIPS R10K processor machine. See the comparison given in table 2.

2.2. Two circular dielectric cylinders

In the next example we consider two circular dielectric cylinders of the same type as in the previous example. The first cylinder is centred at $x = 0$ mm and $y = 45$ mm and the second is centred at $x = -10$ mm and $y = -45$ mm. The actual position of the target is given in figure 2(*a*). The distance between the centres is 90.55 mm, which is approximately three times the diameter of one cylinder. Figures 2(*b*)–(*d*) show the inversion results for DT, MGF and CSIW, respectively. The DT result in figure 2(*b*) reproduces the position and the shape correctly. But one can recognize some ghost targets between the two cylinders. These ghost targets disappear almost in the MGF reconstruction (see figure 2(*c*)). Only the CSIW method gives a clear image of the two cylinders without any ghost targets. The reconstructed maximal contrast value of the DT and MGF is within the given tolerance, only the maximal contrast of the CSIW is above the specified tolerance. Note that we did not apply the RGA to this target configuration, because the computational time can be estimated with one week on a MIPS R10K processor machine. But, in principle, RGA can handle this type of target as well.

2.3. Centred rectangular metallic cylinder

The next scatterer under consideration is a metallic target (perfect scatterer). The actual geometry is given in figure 3(*a*). It is a 'centred' rectangular metallic cylinder with the dimensions 12.7 mm $\times$ 25.4 mm and the centre at $x = -5$ mm and $y = -7.5$ mm. (We note that the cylinder is not perfectly centred.) The inversion results of DT, MGFM, CSIW, and RGA are given in figures 3(*b*)–(*e*). The DT result in figure 3(*b*) is generated for the 16 GHz ($\lambda = 18.75$ mm) data set. Both sides of the scatterer are approximately of the order of 1λ (more accurately, $0.67\lambda \times 1.35\lambda$). Despite the fact that the DT image of the rectangle is quite blurred, the figure still represents the outer contour of the original shape clearly. But the interior of the cylinder is filled with a strong interference pattern, which is also weakly visible outside the scatterer. We note that the interior of the perfect scatterer should be field-free. The results of MGFM and CSIW are given in figures 3(*c*) and (*e*), where we used the backpropagated contrast as the initial guess and the frequency-hopping mode for the 4, 8, 12 and 16 GHz data set. Both images display the contour of the scatterer very sharply. We observe in the MGF result an irregularly broken contour while the CSIW result shows a continuously closed contour. We note that the inside of the reconstructed object appears in the shape of the number '8'. Even the RGA result in figure 3(*e*) for the 16 GHz data set displays this fact. But this comes from a different reason. This is due to the cubic B-spline representation of the shape function, which is not able to represent sharp edges. Despite this drawback, we observe that the RGA result represents the position and size of the metallic target very nicely.

2.4. Decentred rectangular metallic cylinder

In the following example we study the effectiveness of the inversion algorithms applied to scattering data of a considerably decentred target. We make use of the same target type as in the previous case, only the centre is shifted to $(x, y) = (0, 43)$ mm. The actual position

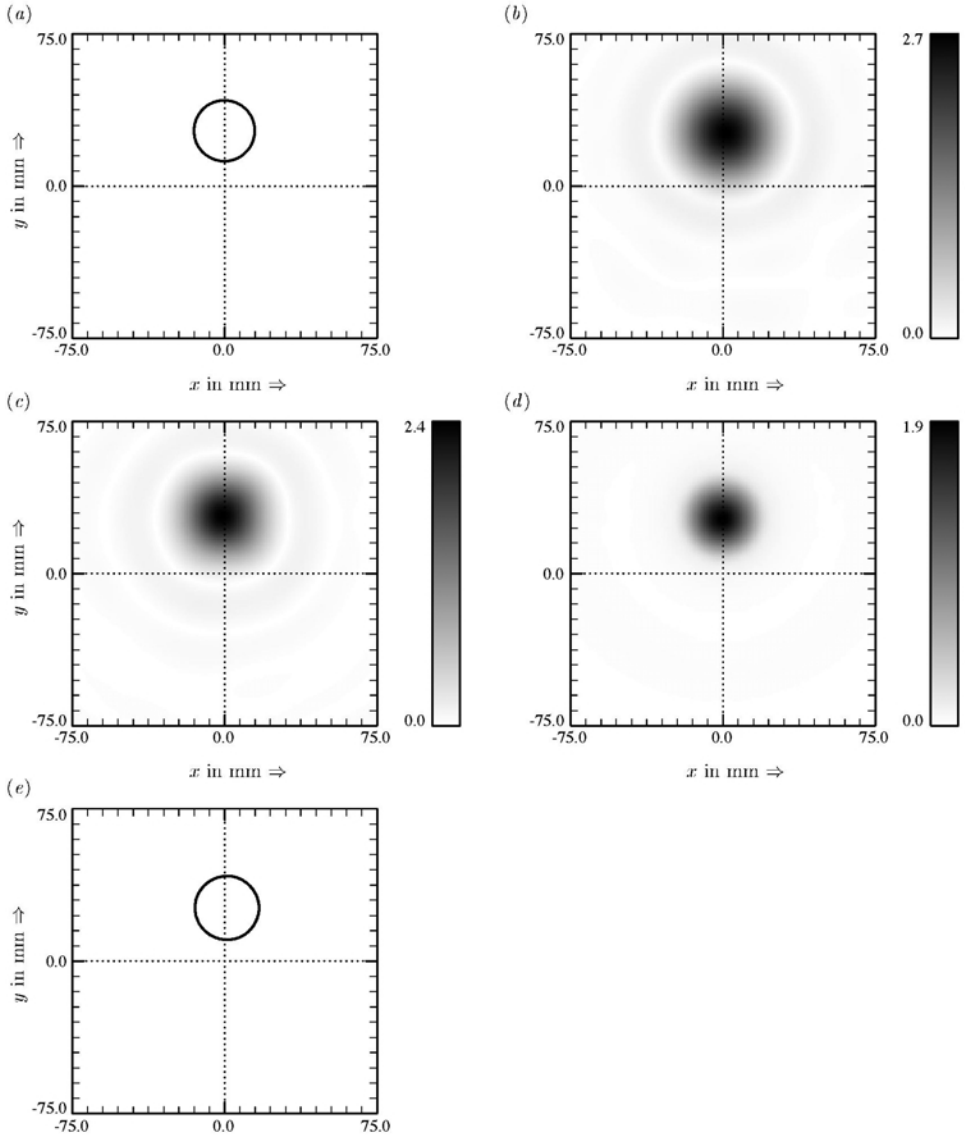

Figure 1. Inversion results for the single circular dielectric cylinder (dielTM_dec8f.exp data set). (*a*) Actual shape and position of the dielectric object with a homogeneous contrast of $\chi = 2.0$. (*b*) Reconstructed contrast using the linear DT algorithm at 8 GHz. (*c*) MGF reconstruction of the contrast with backpropagated contrast as the initial guess using the first four frequencies 1, 2, 3 and 4 GHz simultaneously. (*d*) CSIW reconstruction of the contrast with backpropagated contrast as the initial guess using the first four frequencies 1, 2, 3 and 4 GHz simultaneously. (*e*) RGA reconstruction result of the contrast at 8 GHz. The reconstructed contrast is $\chi = 2.3$. All figures display an area of 150 mm $\times$ 150 mm or in wavelength $4\lambda \times 4\lambda$ at a centre frequency of 8 GHz in free space (background material). In (*b*), (*c*) and (*d*) the magnitude of the material contrast ($\propto$ permittivity) is plotted using a grey scale with 256 levels.

is displayed in figure 4(*a*). The inverse scattering results of all four algorithms are presented in figures 4(*b*)–(*e*). We observe that all reconstructions are not as good as for the centred case in figures 3(*b*)–(*e*). For example, the reconstructed target in the DT results at 16 GHz

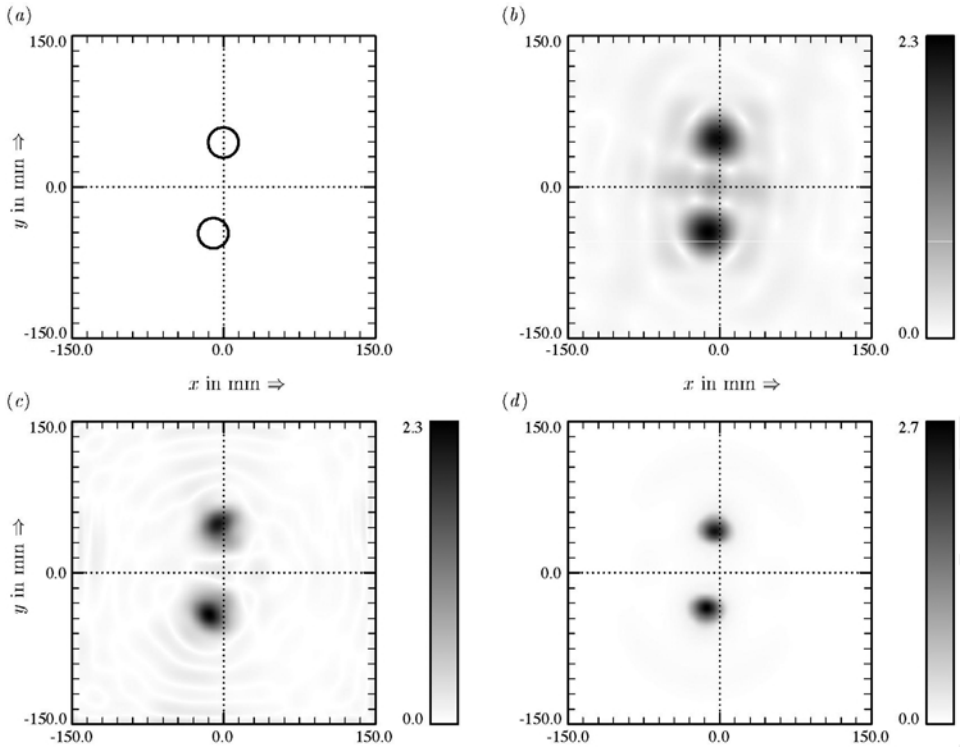

Figure 2. Inversion results for the two identical circular dielectric cylinders (twodielTM_8f.exp data set). (*a*) The actual shape and position of the two dielectric cylinders with a homogeneous contrast of $\chi = 2.0$. (*b*) Linear DT reconstruction of the contrast at 8 GHz. (*c*) MGF reconstruction of the contrast with backpropagated contrast as the initial guess using the first four frequencies 1, 2, 3 and 4 GHz simultaneously. (*d*) CSIW reconstruction of the contrast with backpropagated contrast as the initial guess using the first four frequencies 1, 2, 3 and 4 GHz simultaneously. All figures display an area of 300 mm $\times$ 300 mm or in wavelength $8\lambda \times 8\lambda$ at a centre frequency of 8 GHz in free space (background material). In (*b*), (*c*) and (*d*) the magnitude of the material contrast ($\propto$ permittivity) is plotted using a grey scale with 256 levels.

($\lambda = 18.75$ mm) is still a rectangle, but the upper part of the contour is weaker than the lower part. Then, the MGFM and CSIW results in figures 4(*c*) and (*d*) calculated in frequency-hopping mode for the frequencies 4, 8, 12 and 16 GHz data sets describe a stepped and blurred contour. We remark that we still obtain a clean image. The RGA result in figure 4(*e*), which has been computed for the 16 GHz data set, is, besides the new position, noticeably almost the same as in the centred case (see figure 3(*e*)).

2.5. U-shaped metallic cylinder

The last example is an open metallic cylinder in U-form with the dimensions 80 mm $\times$ 50 mm centred at the origin of the coordinate system (see figure 5(*a*)). The thickness of the metallic walls is unknown. Figure 5(*b*) documents the DT result for the 16 GHz ($\lambda = 18.75$ mm) data set. The size of the displayed area is 150 mm $\times$ 150 mm or $8\lambda \times 8\lambda$ at 16 GHz and the size of the target is $4.27\lambda \times 2.67\lambda$ at 16 GHz. The outer contour of the 'U' and the opening to the right is well reproduced, but the interior as well as the surrounding of the scatterer is filled with an artificial interference pattern. In figures 5(*c*) and (*d*) the MGFM and CSIW results

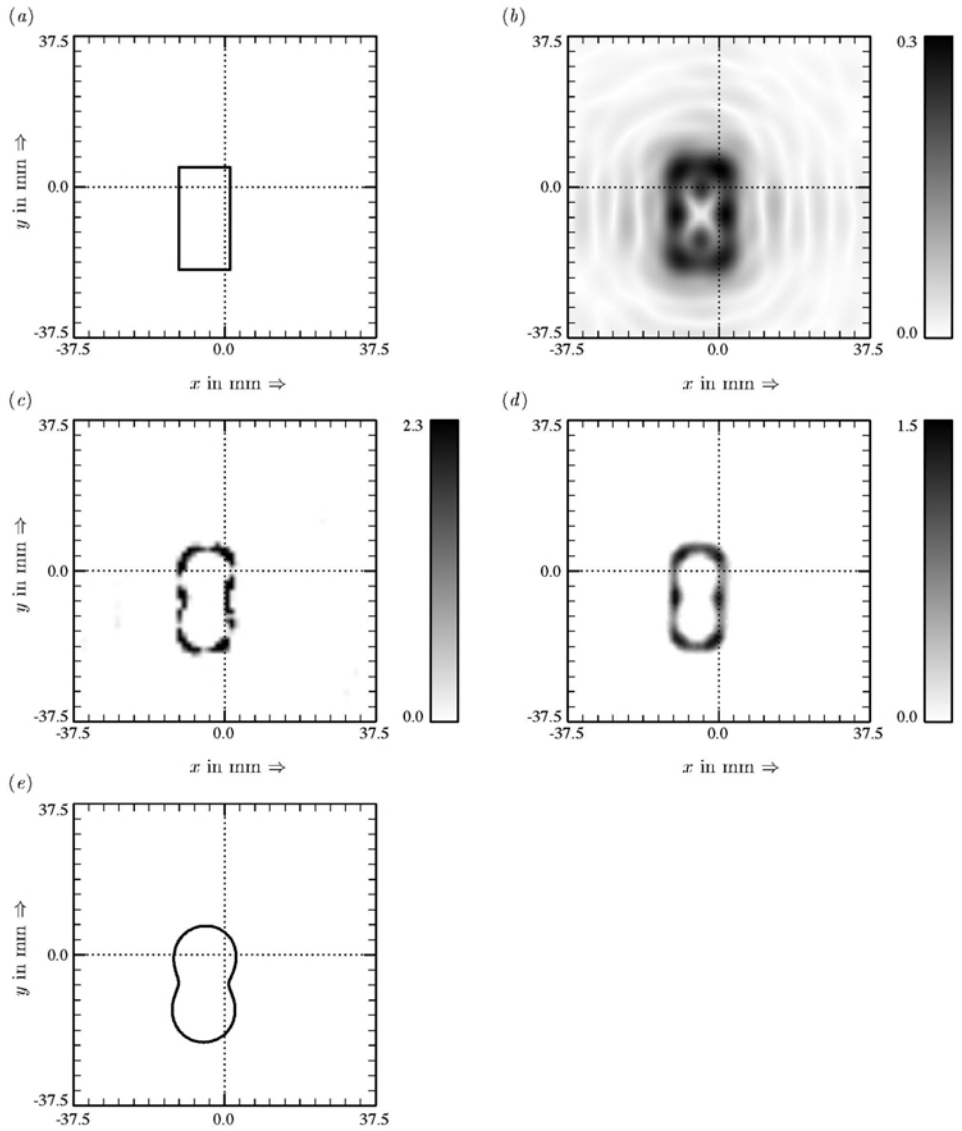

Figure 3. Inversion results for the centred metallic rectangular cylinder (rectTM_cent.exp data set). (*a*) The actual shape and position of the metallic cylinder. (*b*) Reconstructed object using the linear DT algorithm at 16 GHz. (*c*) MGFM reconstruction of the contrast with backpropagated contrast as the initial guess using four frequencies 4, 8, 12 and 16 GHz in frequency-hopping mode. (*d*) CSIW reconstruction of the contrast with backpropagated contrast as the initial guess using four frequencies 4, 8, 12 and 16 GHz in frequency-hopping mode. (*e*) RGA reconstruction result of the shape and position at 16 GHz. All figures display an area of 75 mm × 75 mm or in wavelength 4λ × 4λ at a centre frequency of 16 GHz in free space (background material). In (*b*), (*c*) and (*d*) the magnitude of the material contrast ($\propto$ electric conductivity) is plotted using a grey scale with 256 levels.

are presented. In both cases the frequency-hopping mode using the frequencies 4, 8, 12 and 16 GHz are applied. The nonlinear iterative schemes are able to recover the U-shaped target. Only at the opening to the right is an elliptical lens-shaped artefact present. The RGA result

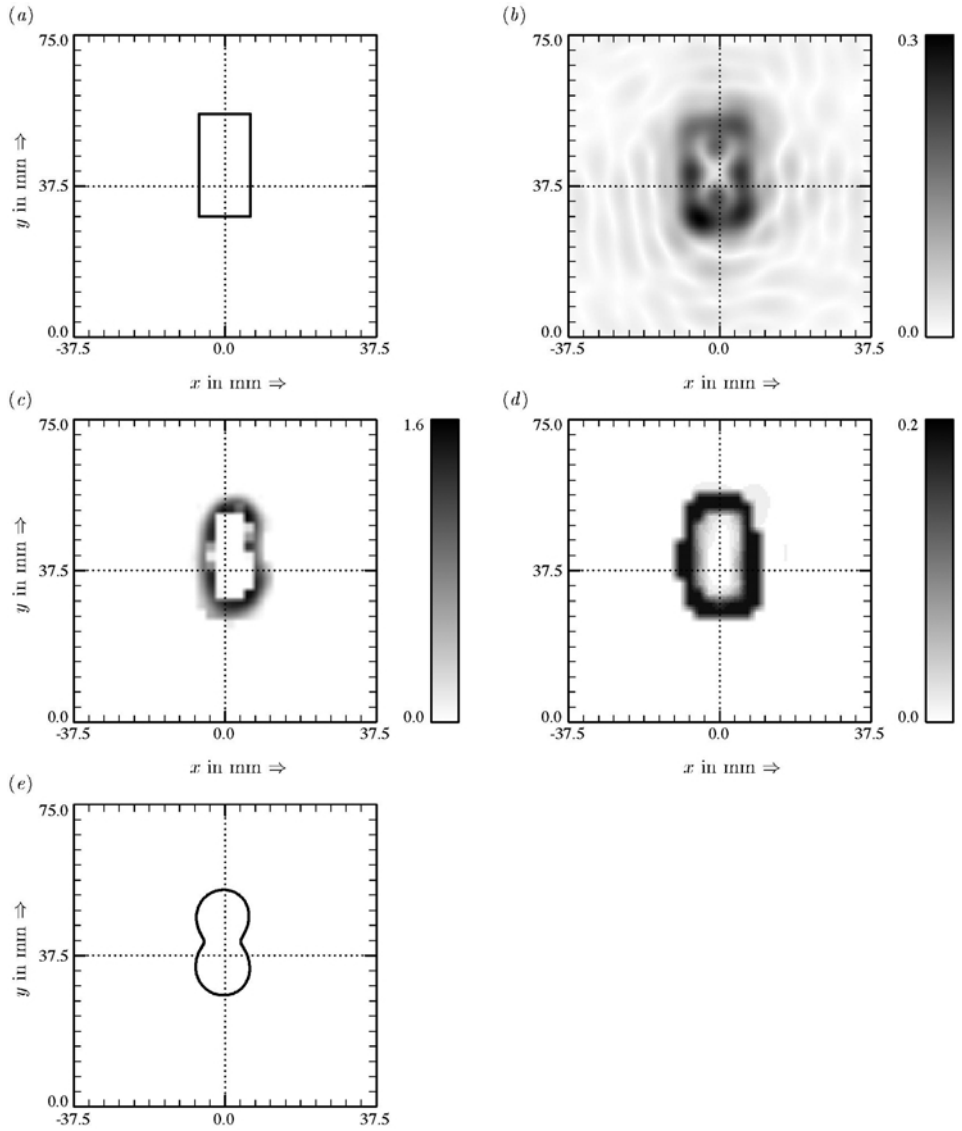

Figure 4. Inversion results for the decentred metallic rectangular cylinder (rectTM_dece.exp data set). (*a*) The actual shape and position of the decentred metallic cylinder. (*b*) Reconstructed object using the linear DT algorithm at 16 GHz. (*c*) MGFM reconstruction of the contrast with backpropagated contrast as the initial guess using four frequencies 4, 8, 12 and 16 GHz in frequency-hopping mode. (*d*) CSIW reconstruction of the contrast with backpropagated contrast as the initial guess using four frequencies 4, 8, 12 and 16 GHz in frequency-hopping mode. (*e*) RGA reconstruction result of the shape and position at 16 GHz. All figures display an area of 75 mm × 75 mm or in wavelength 4λ × 4λ at a centre frequency of 16 GHz in free-space (background material). In (*b*), (*c*) and (*d*) the magnitude of the material contrast ($\propto$ electric conductivity) is plotted using a grey scale with 256 levels.

is also missing for this target, because the currently implemented code is using a local shape function-based approach, which is not able to handle this target type. The handling of targets

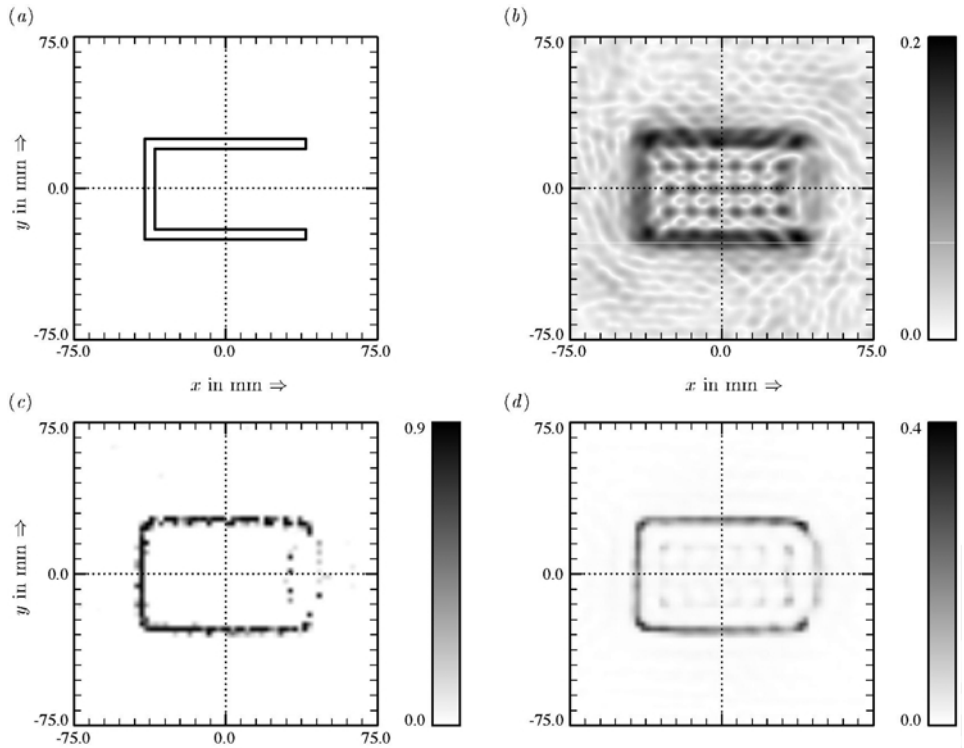

Figure 5. Inversion results for the U-shaped metallic cylinder (uTM_cent.exp data set). (*a*) The actual shape and position of the U-shaped metallic cylinder. (*b*) Reconstructed contrast using the linear DT algorithm at 16 GHz. (*c*) MGFM reconstruction of the contrast with backpropagated contrast as the initial guess using four frequencies 4, 8, 12 and 16 GHz in frequency-hopping mode. (*d*) CSIW reconstruction of the contrast with backpropagated contrast as the initial guess using four frequencies 4, 8, 12 and 16 GHz in frequency-hopping mode. All figures display an area of 150 mm $\times$ 150 mm or in wavelength $8\lambda \times 8\lambda$ at a centre frequency of 16 GHz in free space (background material). In (*b*)–(*d*) the magnitude of the material contrast ($\propto$ electric conductivity) is plotted using a grey scale with 256 levels.

whose contour cannot be modelled by a single-value local shape function will be an aspect to be examined in the future.

2.6. Comparison of convergence of the MGF and CSIW methods

Figure 6 presents a comparison of convergence between MGF and CSIW. Figure 6(*a*) shows the results for the single circular dielectric cylinder as considered in figure 1 and figure 6(*b*) reports the results for the two circular dielectric cylinders as given in figure 2. Here, two different initial guesses for the MGF method have been considered: (i) zero contrast and (ii) backpropagated contrast. It can be observed that the initial guess plays an important role in the convergence of the algorithm. Figure 6 shows that, with the backpropagated contrast as the initial guess, the MGF performs better in comparison with a zero contrast initial guess. Comparing the MGF and CSIW results, it can be seen that the overall convergence and reconstruction for the CSIW is surely better than that of the MGF.

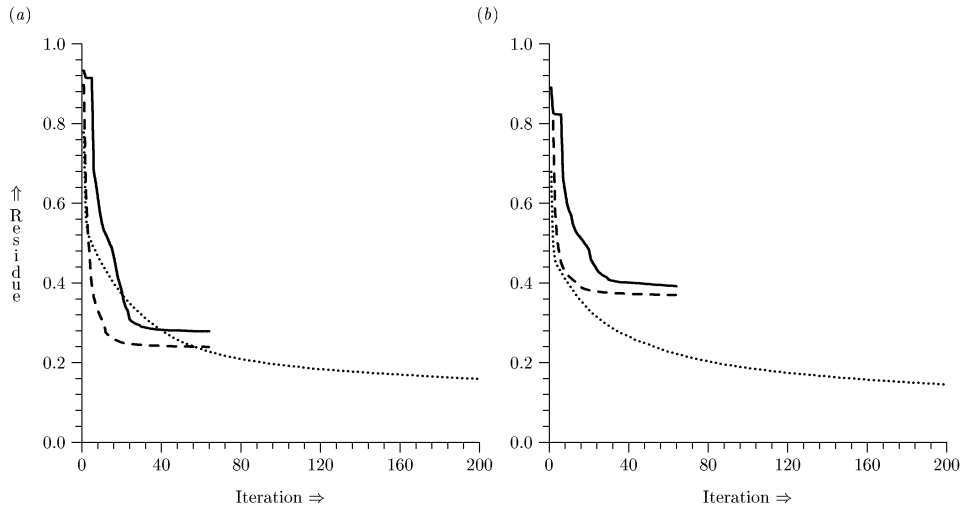

Figure 6. Comparison of the convergence, the residual error as a function of iteration performed, for the (*a*) single dielectric cylinder and (*b*) two identical dielectric cylinders. Legend: —— MGF with zero contrast as initial guess; - - - -MGF for the same parameters as for (*a*) figure 1(*c*) and (*b*) figure 2(*c*); ..... CSIW for the same parameters as for (*a*) figure 1(*d*) and (*b*) figure 2(*d*).

3. Conclusion

We have presented, compared and validated results of linear and nonlinear iterative scalar inversion schemes applied to measured scattering data, which have been recorded in an anechoic chamber in a controlled environment. The results achieved with the nonlinear schemes are much better than those obtained with the linear DT scheme. Nevertheless, it has been shown that even the linear DT scheme of Born type is able to give reasonable results for the dielectric targets (penetrable scatterers) as well as the metallic targets (perfect scatterers). The great advantage of linear schemes is their speed. A quasi real-time processing is achievable. The best results are obtained with the contrast source inversion scheme using weighted sources (CSIW). The second best reconstructions are achieved with the modified gradient in field methods MGF and MGFM. The RGA results suffer from the smooth assumption of the cylinder contour, but this can be avoided by using a more appropriate shape function. For example, the RGA result for the single dielectric cylinder is convincing. We remark that the quality of the MGF, MGFM, CSIW and RGA results is quite similar but essentially better compared to the results of the linear DT scheme. Significant improvements of the reconstructions can be achieved with the presented nonlinear iterative inversion schemes.

Acknowledgments

The authors would like to thank Marc Saillard and Kamal Belkebir from the Institut Fresnel, UMR-CNRS, Marseille, France for the measurements provided and for the invitation to contribute to this special section.

References

Belkebir K, Bonnard S, Pezin F, Sabouroux P and Saillard M 2000 Validation of 2D inverse scattering algorithms from multi-frequency experimental data *J. Electromagn. Waves Appl.* **14** 1637–68

Belkebir K and Saillard M 2001 Special section: Testing inversion algorithms against experimental data *Inverse Problems* **17** 1565–71

Haak K F I 1999 *Multi-Frequency Nonlinear Profile Inversion Methods* (Delft: Delft University Press)

Hofmann Ch 1999 *Lineare und nichtlineare skalare inverse Beugungstheorie* (Aachen: Shaker)

Kleinman R E and van den Berg P M 1992 A modified gradient method for two-dimensional problems in tomography *J. Comput. Appl. Math.* **42** 17–35

—— 1994 Two-dimensional location and shape reconstruction *Radio Sci.* **29** 1157–69

—— 1997 A contrast source inversion method *Inverse Problems* **13** 1607–20

Langenberg K J 1987 Applied inverse problems for acoustic, electromagnetic and elastic wave scattering *Basic Methods of Tomography and Inverse Problems* ed P C Sabatier (Bristol: Adam Hilger) pp 125–467

—— 2001 Linear scalar inverse scattering *Scattering: Scattering and Inverse Scattering in Pure and Applied Sciences* ed E R Pike and P C Sabatier (London: Academic) pp 121–41

Morbitzer H 1991 *Untersuchung von Ultraschallabbildungsverfahren mit und ohne linearisierende Annahme vor dem Hintergrund medizinischer Diagnostik* (Kassel: University of Kassel)

Qing A 2001 Microwave imaging of parallel perfectly conducting cylinders with transverse electric scattering data *J. Electromagn. Waves Appl.* **15** 665–85

Qing A and Lee C K 1999 Microwave imaging of a perfectly conducting cylinder using a real-coded genetic algorithm *IEE Proc. Microwaves Antennas Propag.* **146** 421–5

Qing A, Lee C K and Jen L 2001 Electromagnetic inverse scattering of two-dimensional perfectly conducting objects by real-coded genetic algorithm *IEEE Trans. Geosci. Remote Sens.* **39** 665–76

Qing A and Zhong S 1998 Microwave imaging of two-dimensional perfectly conducting objects using real-coded genetic algorithm *IEEE Antennas and Propagation Society International Symp. 1998* vol 2 (Piscataway, NJ: IEEE) pp 726–9

Sabouroux P and Parneix J P 1992 A large bandwidth measurement system for the microwave characterization of absorbing materials *J. Wave–Mater. Interaction* **7** 57–70

Sabouroux P and Pezin F 2000 Experimental scattering data from cylindrical targets for validating inverse scattering algorithms (Marseille Cedex: Institut Fresnel) http://www.loe.u-3mrs.fr Data sets can be downloaded from: http://www.loe.u-3mrs.fr/inverse_scat/data_scat

van den Berg P M 1999 Reconstruction of media posed as an optimization problem *Wavefield Inversion* ed A Wirgin (Wien: Springer) pp 191–240

—— 2001 Non-linear scalar inverse scattering algorithms and applications *Scattering: Scattering and Inverse Scattering in Pure and Applied Sciences* ed E R Pike and P C Sabatier (London: Academic) pp 142–61